Biophysical Journal, Volume 99

Supporting Material

The mechanical properties of PCNA: Implications for the loading and function of a DNA sliding clamp

Joshua L. Adelman, John D. Chodera, I-Feng W Kuo, Thomas F. Miller, III, and Daniel Barsky

Supporting Materials

The mechanical properties of PCNA: Implications for the loading and function of a DNA sliding clamp

Adelman et al.

System Setup and Simulation Protocol

Hydrogen atoms were added to the high-resolution crystal structure of PCNA from budding yeast, Saccharomyces cerevisiae (Protein Data Bank ID code 1PLQ) (1), using the psfGen plug-in in VMD (2), after removal of all non-protein atoms and one of the three subunits of the full trimer. All Lys and Arg residues were protonated and all His, Glu and Asp were deprotonated. The protein was then placed in a box of TIP3 water measuring approximately 68 X 87 X 114 $Å^3$ using SOLVATE, with 0.15 M NaCl (49 Na^+ and 9 Cl^- ions) in proportions that neutralize the system. All simulations were performed using NAMD 2.6 (3) in the NPT ensemble at 300 K and 1 atm, using Langevin Dynamics with the damping coefficient set to 5 ps^{-1} and the Nosé-Hoover Langevin Piston barostat with a decay period of 100 fs and a damping timescale of 50 fs.

All bond lengths to hydrogen atoms were constrained using SHAKE with a tolerance of $1x10^{-10}$ Å. Van der Waals and local electrostatic interactions were cut-off at 10 Å and smoothly switched to zero at 12 Å. Long-range electrostatic interactions were calculated using the Particle Mesh Ewald (PME) method on an 64 X 80 X 128 grid. The equations of motions were integrated using the multiple-timestep RESPA integrator, with a 2 fs time-step, where the electrostatic forces were evaluated every 4 fs. The simulation of the full trimer was performed using the same procedure described for the dimer above, expect the box size (112 X 69 X 115 $Å^3$), number of ions (67 Na^+ and 7 Cl^- ions) and PME grid (120 X 75 X 120) were adjusted to accommodate the geometry of the additional subunit. All simulations used the CHARMM22 protein force-field (4) with CMAP corrections (5) unless noted otherwise.

After 1500 steps of minimization using the conjugate gradient method, the system was heated to 300 K gradually over 0.5 ns, with 5 $kcal \cdot mol^{-1} \cdot Å^{-2}$

harmonic restraints applied to all of the protein heavy-atoms. These restraints were then removed in 0.5 kcal·mol^{-1}·Å^{-2} steps every 100 ps until the protein was no longer restrained in its motion. A separate heating and equilibration phase was performed for each of the four simulations, using a different randomization seed to initialize the atomic velocities and stochastic thermo- and barostats. Production runs of 92, 46, 51 and 48 ns in length were simulated and coordinates of the protein and solvent were recorded every 4 ps.

Two additional simulations of PCNA from yeast were performed using the Amber PARM94 (6) and PARM99SB force-fields (7). They were prepared using the Amber Tools suite v1.2, starting from the same initial PDB file (1) placed in a water box measuring approximately 76 X 120 X 108 Å^3 with 0.15 M NaCl (61Na$^+$ and 21 Cl$^-$ ions). Long-range electrostatic interactions were calculated using the Particle Mesh Ewald (PME) method on an 81 X 125 X 120 grid. All other parameters and protocols are identical to the CHARMM22 simulations.

Two simulations of PCNA from the hyperthermophilic archaeon, *Pyrococcus furiosus* (pfuPCNA) (Protein Data Bank ID code 1GE8) (8) were performed using the same protocol described above for the dimeric yeast PCNA simulations. In the archael clamp, residues 118 –125 in the intra-domain linker were disordered in the crystal structure; this region was built using MODELLER 9v6 (9) based on the structure of these residues in the PCNA from yeast. The dimer was placed in a water box measuring approximately 126 X 94 X 67 Å^3 using SOLVATE, with 0.15 M NaCl (49 Na$^+$ and 13 Cl$^-$ ions) in proportions that neutralize the system. Long-range electrostatic interactions were calculated using the Particle Mesh Ewald (PME) method on an 128 X 96 X 64 grid. Production runs of 38 ns were performed using the CHARMM22 protein force-field (4) with CMAP corrections (5) .

Analysis of the elastic network model and PCA modes

The mean square fluctuations of the individual C$^\alpha$ atoms in the elastic network model can be calculated from the eigenvectors and eigenvalues obtained

from the decomposition of the Hessian of the energy function

$$\left\langle \Delta R_i^2 \right\rangle \backsim \sum_{i=1}^{N} \sum_{k=1}^{3} \frac{v_{ik} v_{ik}}{\lambda_i} \tag{1}$$

where λ_i is the eigenvalue corresponding to mode i and v_{ia} is the a^{th} component of the eigenvector of mode i. and the overlap between two modes i from some subset of modes A and j from some subset of modes B is

$$O_{i.j} = \frac{|A_i \cdot B_j|}{\|A_i\| \|B_j\|} \tag{2}$$

Error Estimation for out-of-plane order parameter

Statistical errors for averages of timeseries data were estimated by autocorrelation analysis (10–12). Normalized fluctuation autocorrelation functions were estimated from the timeseries data and used to compute an integrated autocorrelationtime τ as described in Section 5.2 of (12), except that the contributions to unnormalized autocorrelation functions $\langle A(0)A(t)\rangle$ were accumulated from all trajectories and averaged. The statistical inefficiency $g = 1 + 2\tau$ was used to reduce the total number of correlated samples N from all pooled trajectories to obtain the effective number of uncorrelated samples $N_{\text{eff}} \approx N/g$. The standard deviation of the timeseries data σ was estimated from all samples, and the standard error of the mean estimated from $\sigma/\sqrt{N_{\text{eff}}}$. This computation was performed using the 'timeseries' module of the pyMBAR code, available at http://www.simtk.org/home/pysmbar.

Correspondence between in-plane order parameter and gap size

Kazmirski et al. (13), measured the in-plane opening of their PCNA dimer systems by constructing an artificial trimer (as described in the main text), but instead of calculating the change distance between the centers-of-mass of the domains on either side of the interface, they computed the minimum distance between any atom in one domain and any atom in the other. This

metric provides a better approximation of the gap size induced by a particular conformational change in the dimer, but suffers a major drawback: Since atoms in the virtual subunit do not interact with the simulated system, the virtual domain (3A) can interpenetrate domain 2B, causing an unphysical overlap in atoms. When this occurs, the in-plane order parameter becomes uninterpretable in the context of the gap size, and spurious densities are recorded around the closed state. Conversely, the projected distance between the centers-of-mass of the two domains can increase, but due to the geometry of the system, only a negligible gap forms. To illustrate this point, we plot both the 'minimum distance' and 'projected in-plane displacement' order parameters together in Fig. S1. While the two order parameters are generally correlated, there are regions of conformational space, where the projection onto the one-dimensional order parameters diverge in what physical quantity they are describing. We have chosen the in-plane projected distance, rather than the minimum distance, as the former is physically valid over the entire range of values reported, and is readably transferable to the conformations generated by the C^{α} based ENM. Finally, Fig. S1 shows that although the in-plane distance order parameter we have chosen does not directly report the gap between domains across the open interface, gaps sufficient to allow passage of double-stranded DNA into PCNA's central pore are observed.

Results are robust against variations in force-field

In order to validate the robustness of our results, we performed two additional simulations of the dimer system using different sets of force field parameters. We compare our original simulations with simulations using AMBER PARM 94 and 99SB (6, 7) (see Fig. S2 and SS3, respectively). The former is the force field used in (13), although it has since been deprecated (14). We find that the results obtained with these force fields are qualitatively consistent with the results reported for the in- and out-of-plane order parameters and rms deviations. Echoing previous simulations, our trajectories using the AMBER94 fluctuated primarily in the right-handed direction during the first 10 ns, but this short time scale preference appears to be either a transient fluctuation or part of the relaxation phase of the molecule following removal of the closure constraint.

Conformational fluctuations of a closed PCNA trimer

As described in the main text, we have simulated a full trimer of yPCNA in its closed state in order to determine to what extent the closure of the ring restricts the motions of the subunits. We have calculated the fluctuations along the in- and out-of-plane coordinates for the full trimer as shown in Fig. S5. In calculating these quantities, we are address the fluctuations of subunits 1 and 2 within the trimer. While the ring remains closed (all inter-subunit contacts are retained), the in-plane fluctuations report on the flexibility of a subset of the domains in the in-plane direction, rather than reflecting an approximation of a gap. The comparison of the observed distributions in conformations for the dimeric and trimeric systems, projected onto the in- and out-of-plane order parameters is shown in Figs. S5C and D. The comparison of in-plane distances for the two oligomeric states of PCNA show that the presence of the third subunit, dramatically constrains the fluctuations of the other two subunits. This indicates that while the interface causes the ring to be stable in the closed state, the packing of the three subunits into the ring causes a circumferential stress that restricts the conformational fluctuations of individual subunits in-plane. As mentioned in the main text, subunits 1 and 2 are able to fluctuate out-of-plane, both above and below the plane, showing that right- and left-handed conformations are also accessible in the closed form of PCNA. Again, the motions are restricted compared to the isolated dimer.

References

[1] Krishna, T. S., X. P. Kong, S. Gary, P. M. Burgers, and J. Kuriyan, 1994. Crystal structure of the eukaryotic DNA polymerase processivity factor PCNA. *Cell* 79:1233–1243.

[2] Humphrey, W., A. Dalke, and K. Schulten, 1996. VMD: visual molecular dynamics. *J Mol Graph* 14:33–8, 27–8.

[3] Phillips, J. C., R. Braun, W. Wang, J. Gumbart, E. Tajkhorshid, E. Villa, C. Chipot, R. D. Skeel, L. Kalé, and K. Schulten, 2005. Scalable molecular dynamics with NAMD. *J Comput Chem* 26:1781–802.

[4] MacKerell, A. D., D. Bashford, Bellott, R. L. Dunbrack, J. D. Evanseck, M. J. Field, S. Fischer, J. Gao, H. Guo, S. Ha, D. Joseph-McCarthy, L. Kuchnir, K. Kuczera, F. T. K. Lau, C. Mattos, S. Michnick, T. Ngo, D. T. Nguyen, B. Prodhom, W. E. Reiher, B. Roux, M. Schlenkrich, J. C. Smith, R. Stote, J. Straub, M. Watanabe, J. Wiorkiewicz-Kuczera, D. Yin, and M. Karplus, 1998. All-Atom Empirical Potential for Molecular Modeling and Dynamics Studies of Proteins. *The Journal of Physical Chemistry B* 102:3586–3616.

[5] Mackerell, A. D., Jr, M. Feig, and C. L. Brooks, 3rd, 2004. Extending the treatment of backbone energetics in protein force fields: limitations of gas-phase quantum mechanics in reproducing protein conformational distributions in molecular dynamics simulations. *J Comput Chem* 25:1400–15.

[6] Cornell, W., P. Cieplak, C. I. Bayly, K. Gould, D. Ferguson, D. Spellmeyer, T. Fox, J. Caldwell, and P. Kollman, 1995. A Second Generation Force Field for the Simulation of Proteins, Nucleic Acids, and Organic Molecules. *Journal of the American Chemical Society* 117:5179–5197.

[7] Hornak, V., R. Abel, A. Okur, B. Strockbine, A. Roitberg, and C. Simmerling, 2006. Comparison of multiple Amber force fields and development of improved protein backbone parameters. *Proteins* 65:712–25.

[8] Matsumiya, S., Y. Ishino, and K. Morikawa, 2001. Crystal structure of an archaeal DNA sliding clamp: proliferating cell nuclear antigen from Pyrococcus furiosus. *Protein Sci* 10:17–23.

[9] Sali, A., and T. L. Blundell, 1993. Comparative protein modelling by satisfaction of spatial restraints. *J Mol Biol* 234:779–815.

[10] Swope, W. C., H. C. Andersen, P. H. Berens, and K. R. Wilson, 1982. A computer simulation method for the calculation of equilibrium constants for the formation of physical clusters of molecules: Application to small water clusters. *J. Chem. Phys.* 76:637–649.

[11] Janke, W., 2002. Statistical analysis of simulations: Data correlations and error estimation. *In* J. Grotendorst, D. Marx, and A. Murmatsu, editors, Quantum Simulations of Complex Many-Body Systems: From

Theory to Algorithms, John von Neumann Institute for Computing, volume 10, 423–445.

[12] Chodera, J. D., W. C. Swope, J. W. Pitera, C. Seok, and K. A. Dill, 2007. Use of the weighted histogram analysis method for the analysis of simulated and parallel tempering simulations. *J. Chem. Theor. Comput.* 3:26–41.

[13] Kazmirski, S. L., Y. Zhao, G. D. Bowman, M. O'donnell, and J. Kuriyan, 2005. Out-of-plane motions in open sliding clamps: molecular dynamics simulations of eukaryotic and archaeal proliferating cell nuclear antigen. *Proc Natl Acad Sci U S A* 102:13801–13806.

[14] Case, D. A., 2008. AmberTools Users' Manual, 1.0 edition.

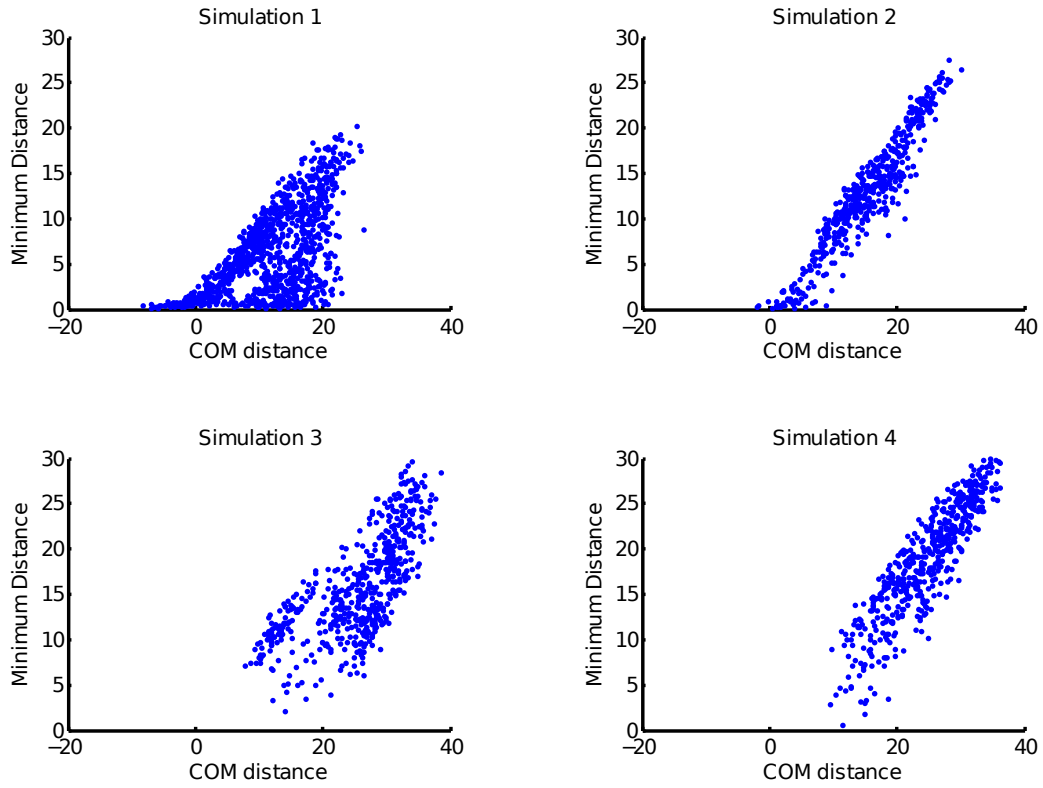

Figure S1: Comparison of in-plane distance order parameters. In-plane order parameters were calculated for the four main simulations of dimeric PCNA from yeast. While both order parameters are correlated, there are regions of conformational space where the two metrics breakdown in their agreement.

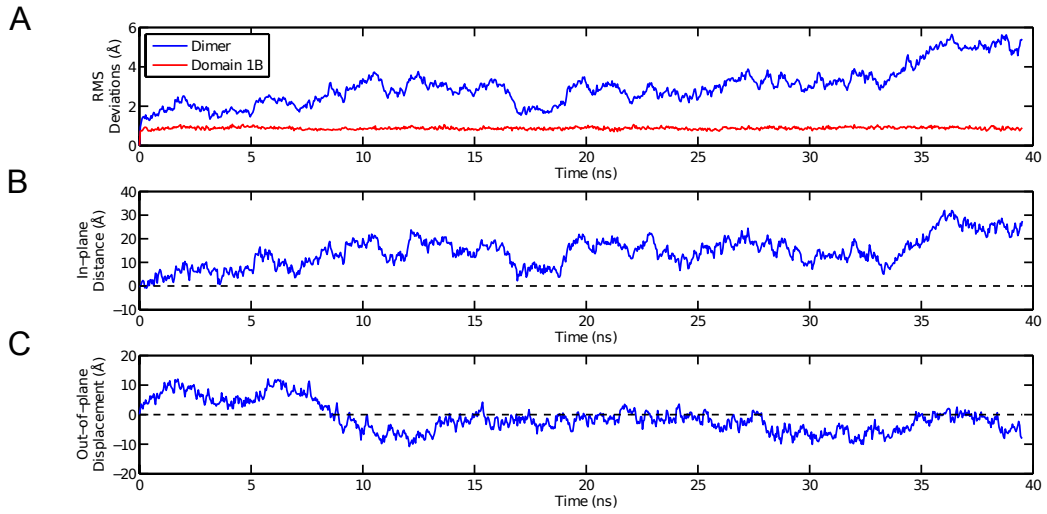

Figure S2: Summary of simulation run with the Amber94 force-field. (A) The rms deviations in C^{α} positions from the crystal structure. The dimer rapidly diverges from its starting conformation in both simulations, however individual domains display small deviations when superimposed individually. The rms deviations of domain 1B (residues 132-183, 195-253) are less than 1 Å over the entire simulation. The other three domains display similar rms deviations. (B) In-plane displacements as a function of time. With the Amber94 force-field, as with our main simulations using CHARMM22 with CMAP corrections, the dimer relaxes to adopt to adopt a more open conformation. (C) Out-of-plane displacement as a function of time. The dimer in this simulation transiently fluctuates in the right-handed direction over the first 10 ns, but then samples conformations with a left-handed spiral as well.

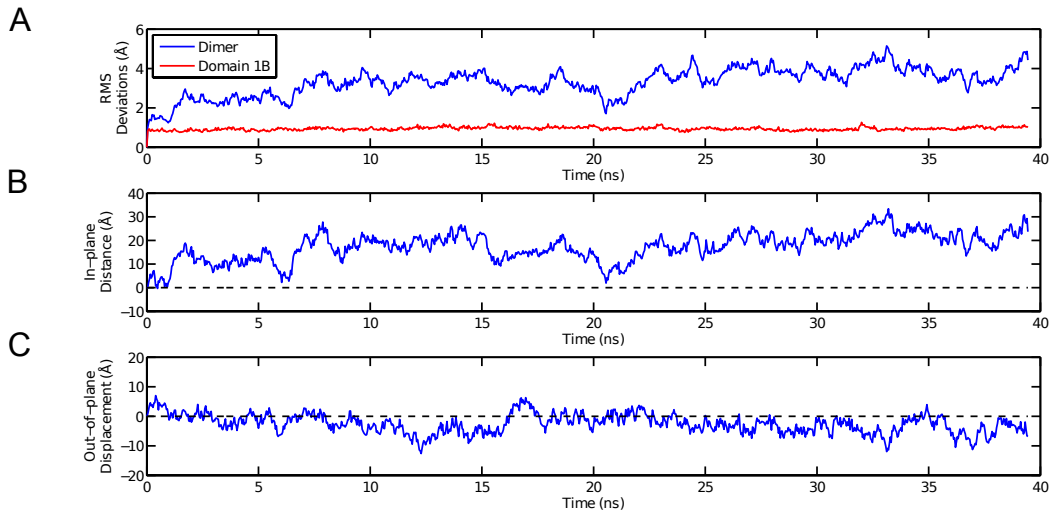

Figure S3: Summary of simulation run with the Amber99sb force-field. (A) The rms deviations in C^{α} positions from the crystal structure. The dimer rapidly diverges from its starting conformation in both simulations, however individual domains display small deviations when superimposed individually. The rms deviations of domain 1B (residues 132-183, 195-253) are less than 1 Å over the entire simulation. The other three domains display similar rms deviations. (B) In-plane displacements as a function of time. With the Amber99sb force-field, as with our main simulations using CHARMM22 with CMAP corrections, the dimer relaxes to adopt to adopt a more open conformation. (C) Out-of-plane displacement as a function of time.

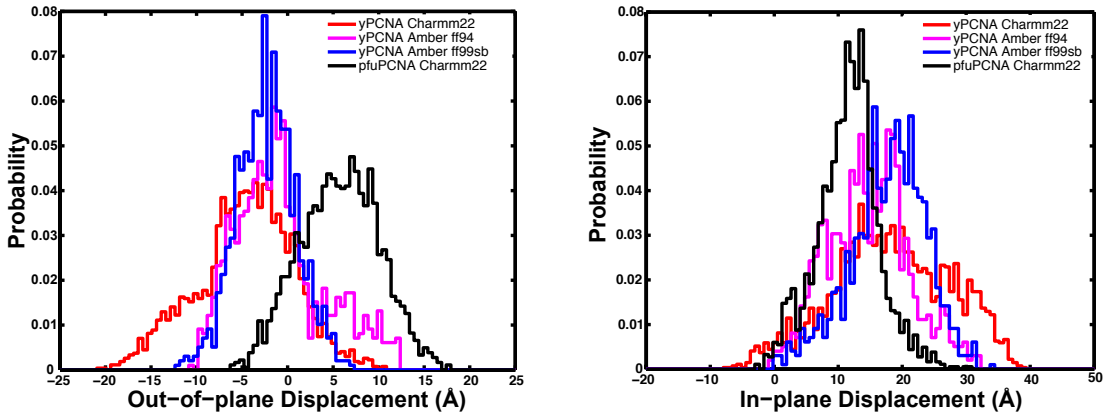

Figure S4: A comparison of In- and Out-of-plane conformations of PCNA from yeast and pfuPCNA. (A) Histogram of the out-of-plane distribution of conformations for yPCNA performed with the Charmm22 forcefield (red), Amber ff94 (magenta), Amber 99sb (blue), and pfuPCNA (black) performed with the Charmm22 forcefield. (B) Histogram of the in-plane distribution of conformations. The coloring scheme in B is identical to A.

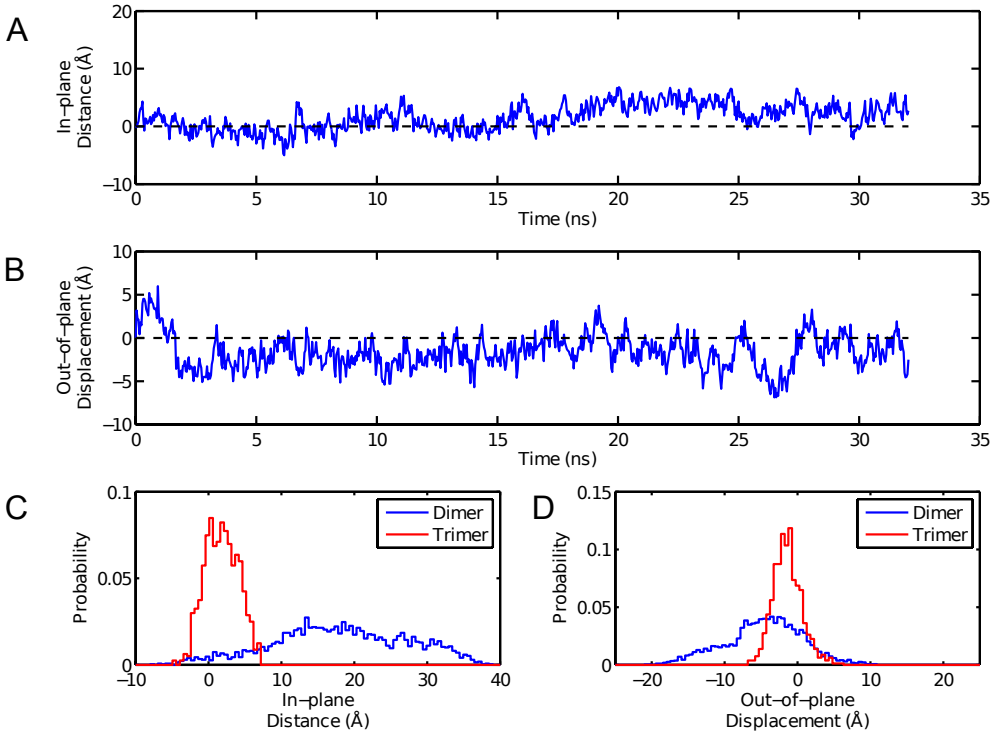

Figure S5: Conformational fluctuations of a closed PCNA trimer. (A) In-plane fluctuations of subunits 1 and 2 within the trimer. (B) Out-of-plane fluctuations of subunits 1 and 2 within the trimer. (C) Distribution of observed in-plane distances compared to those observed for the PCNA dimer. (D) Distribution of out-of-plane displacements compared to those observed in the PCNA dimer.

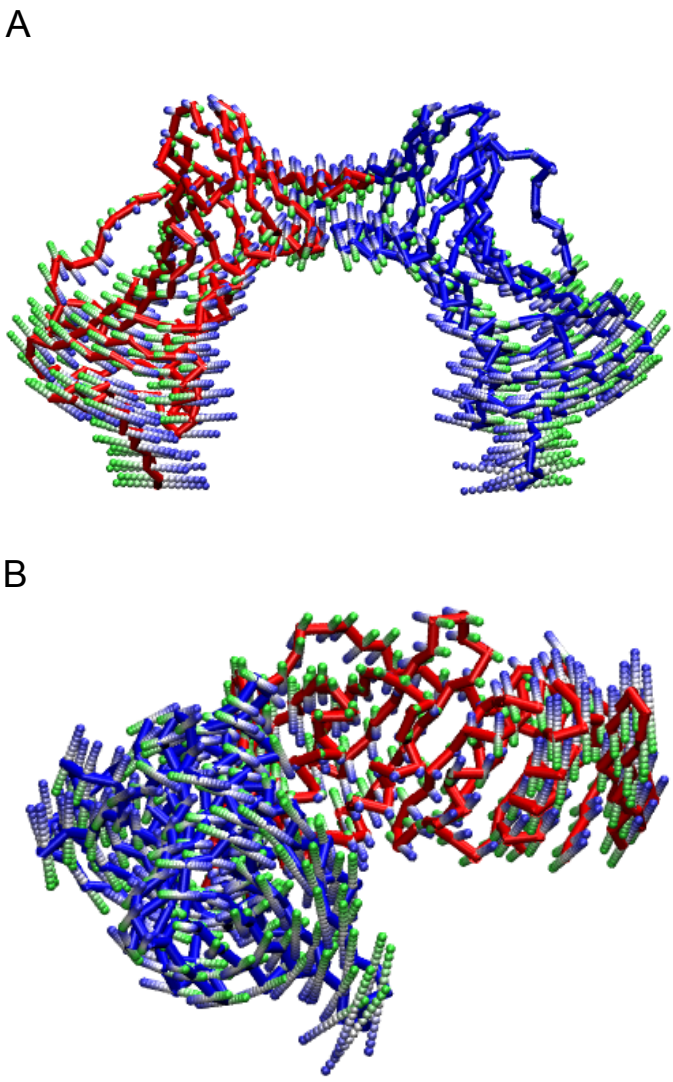

Figure S6: Collective modes of PCNA deformation derived using PCA. (A) The first mode corresponds to a bending motion of the β-sheet at the subunit subunit interface. (B) Twisting of the same structural motif dominates the second mode. A porcupine plot of the vectors along which the protein deforms is overlaid on the trace of the C^{α} atoms. The vectors are color coded according to the magnitude of the projection along mode.

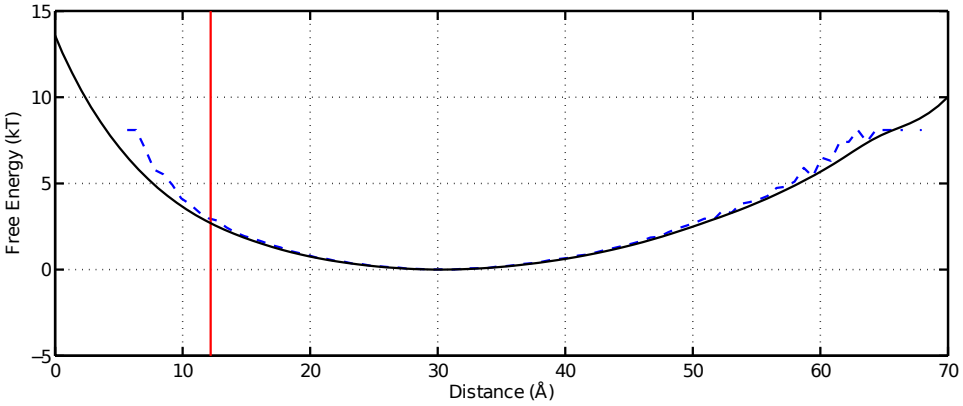

Figure S7: One-dimensional potential of mean force for the distance between a pair of residues across the open interface. The potential of mean force (PMF) for the separation distance between residue 107 in domain 3A and 185 in domain 2B. The distance between these residues in the crystal structure is 12 Å (denoted by the red vertical line). The PMF estimated using the kernel density method with $\sigma = 2$ Å is shown as the solid black line; The PMF from the raw histogram of distances is shown as the dashed blue line.